SLAC-PUB-14018

A change in the optical polarization associated with a γ-ray flare in the blazar 3C 279

A. A. Abdo[1,2], M. Ackermann[3], M. Ajello[3], M. Axelsson[4,5], L. Baldini[6], J. Ballet[7], G. Barbiellini[8,9], D. Bastieri[10,11], B. M. Baughman[12], K. Bechtol[3], R. Bellazzini[6], B. Berenji[3], R. D. Blandford[3], E. D. Bloom[3], D. C.-J. Bock[13,14], J. R. Bogart[3], E. Bonamente[15,16], A. W. Borgland[3], A. Bouvier[3], J. Bregeon[6], A. Brez[6], M. Brigida[17,18], P. Bruel[19], T. H. Burnett[20], S. Buson[10], G. A. Caliandro[21], R. A. Cameron[3], P. A. Caraveo[22], J. M. Casandjian[7], E. Cavazzuti[23], C. Cecchi[15,16], Ö. Çelik[24,25,26], A. Chekhtman[1,27], C. C. Cheung[1,2], J. Chiang[3], S. Ciprini[16], R. Claus[3], J. Cohen-Tanugi[28], W. Collmar[29], L. R. Cominsky[30], J. Conrad[31,5,32], S. Corbel[7,33], R. Corbet[24,26], L. Costamante[3], S. Cutini[23], C. D. Dermer[1], A. de Angelis[34], F. de Palma[17,18], S. W. Digel[3], E. do Couto e Silva[3], P. S. Drell[3], R. Dubois[3], D. Dumora[35,36], C. Farnier[28], C. Favuzzi[17,18], S. J. Fegan[19], E. C. Ferrara[24], W. B. Focke[3], P. Fortin[19], M. Frailis[34,37], L. Fuhrmann[38], Y. Fukazawa[39], S. Funk[3], P. Fusco[17,18], F. Gargano[18], D. Gasparrini[23], N. Gehrels[24,40,41], S. Germani[15,16], B. Giebels[19], N. Giglietto[17,18], P. Giommi[23], F. Giordano[17,18], M. Giroletti[42], T. Glanzman[3], G. Godfrey[3], I. A. Grenier[7], J. E. Grove[1], L. Guillemot[38,35,36], S. Guiriec[43], Y. Hanabata[39], A. K. Harding[24], M. Hayashida[3], E. Hays[24], D. Horan[19], R. E. Hughes[12], G. Iafrate[8,37], R. Itoh[39], M. S. Jackson[44,5], G. Jóhannesson[3], A. S. Johnson[3], W. N. Johnson[1], M. Kadler[45,25,46,47], T. Kamae[3], H. Katagiri[39], J. Kataoka[48], N. Kawai[49,50], M. Kerr[20], J. Knödlseder[51], M. L. Kocian[3], M. Kuss[6], J. Lande[3], S. Larsson[31,5], L. Latronico[6], M. Lemoine-Goumard[35,36], F. Longo[8,9], F. Loparco[17,18], B. Lott[35,36], M. N. Lovellette[1], P. Lubrano[15,16], J. Macquart[52], G. M. Madejski[3], A. Makeev[1,27], W. Max-Moerbeck[53], M. N. Mazziotta[18], W. McConville[24,41], J. E. McEnery[24,41], S. McGlynn[44,5], C. Meurer[31,5], P. F. Michelson[3], W. Mitthumsiri[3], T. Mizuno[39], A. A. Moiseev[25,41], C. Monte[17,18], M. E. Monzani[3], A. Morselli[54], I. V. Moskalenko[3], S. Murgia[3], I. Nestoras[38], P. L. Nolan[3], J. P. Norris[55], E. Nuss[28], T. Ohsugi[39], A. Okumura[56], N. Omodei[6], E. Orlando[29], J. F. Ormes[55], D. Paneque[3], J. H. Panetta[3], D. Parent[1,27,35,36], V. Pavlidou[53], T. J. Pearson[53], V. Pelassa[28], M. Pepe[15,16], M. Pesce-Rollins[6], F. Piron[28], T. A. Porter[57], S. Rainò[17,18], R. Rando[10,11], M. Razzano[6], A. Readhead[53], A. Reimer[58,3], O. Reimer[58,3], T. Reposeur[35,36], L. C. Reyes[59], J. L. Richards[53], L. S. Rochester[3], A. Y. Rodriguez[21], M. Roth[20], F. Ryde[44,5], H. F.-W. Sadrozinski[57], D. Sanchez[19], A. Sander[12], P. M. Saz Parkinson[57], J. D. Scargle[60], C. Sgrò[6], M. S. Shaw[3], C. Shrader[25], E. J. Siskind[61], D. A. Smith[35,36], P. D. Smith[12], G. Spandre[6], P. Spinelli[17,18], L. Stawarz[95,3], M. Stevenson[53], M. S. Strickman[1], D. J. Suson[62], H. Tajima[3], H. Takahashi[39], T. Takahashi[63], T. Tanaka[3], G. B. Taylor[64], J. B. Thayer[3], J. G. Thayer[3], D. J. Thompson[24], L. Tibaldo[10,11,7,65], D. F. Torres[66,21], G. Tosti[15,16], A. Tramacere[3,67], Y. Uchiyama[3], T. L. Usher[3], V. Vasileiou[25,26], N. Vilchez[51], V. Vitale[54,68], A. P. Waite[3], P. Wang[3], A. E. Wehrle[69], B. L. Winer[12], K. S. Wood[1], T. Ylinen[44,70,5], J. A. Zensus[38], M. Ziegler[57] (the *Fermi*-LAT collaboration) and M. Uemura[87], Y. Ikejiri[39], K. S. Kawabata[87], M. Kino[88], K. Sakimoto[39], M. Sasada[39],

SLAC National Accelerator Laboratory, Menlo Park, CA 94025
Work supported in part by US Department of Energy contract DE-AC02-76SF00515.

S. Sato[88], M. Yamanaka[39], M. Villata[93], C. M. Raiteri[93], I. Agudo[71], H. D. Aller[72], M. F. Aller[72], E. Angelakis[38], A. A. Arkharov[73], U. Bach[38], E. Benítez[74], A. Berdyugin[75], D. A. Blinov[75,80], M. Boettcher[76], C. S. Buemi[77], W. P. Chen[78], M. Dolci[79], D. Dultzin[74], N. V. Efimova[73,80], M. A. Gurwell[82], C. Gusbar[76], J. L. Gómez[71], J. Heidt[83], D. Hiriart[84], T. Hovatta[85], S. G. Jorstad[86], T. S. Konstantinova[80], E. N. Kopatskaya[80], E. Koptelova[78], O. M. Kurtanidze[89], A. Lahteenmaki[85], V. M. Larionov[80], E. G. Larionova[80], P. Leto[77], H. C. Lin[78], E. Lindfors[75], A. P. Marscher[86], I. M. McHardy[90], D. A. Melnichuk[80], M. Mommert[83], K. Nilsson[75], A. Di Paola[92], R. Reinthal[75], G. M. Richter[94], M. Roca-Sogorb[71], P. Roustazadeh[76], L. A. Sigua[89], L. O. Takalo[75], M. Tornikoski[85], C. Trigilio[77], I. S. Troitsky[80], G. Umana[77], C. Villforth[75], K. Grainge[81], R. Moderski[91], K. Nalewajko[91], M. Sikora[91]

1. Space Science Division, Naval Research Laboratory, Washington, DC 20375, USA
2. National Research Council Research Associate, National Academy of Sciences, Washington, DC 20001, USA
3. W. W. Hansen Experimental Physics Laboratory, Kavli Institute for Particle Astrophysics and Cosmology, Department of Physics and SLAC National Accelerator Laboratory, Stanford University, Stanford, CA 94305, USA
4. Department of Astronomy, Stockholm University, SE-106 91 Stockholm, Sweden
5. The Oskar Klein Centre for Cosmoparticle Physics, AlbaNova, SE-106 91 Stockholm, Sweden
6. Istituto Nazionale di Fisica Nucleare, Sezione di Pisa, I-56127 Pisa, Italy
7. Laboratoire AIM, CEA-IRFU/CNRS/Université Paris Diderot, Service d'Astrophysique, CEA Saclay, 91191 Gif sur Yvette, France
8. Istituto Nazionale di Fisica Nucleare, Sezione di Trieste, I-34127 Trieste, Italy
9. Dipartimento di Fisica, Università di Trieste, I-34127 Trieste, Italy
10. Istituto Nazionale di Fisica Nucleare, Sezione di Padova, I-35131 Padova, Italy
11. Dipartimento di Fisica "G. Galilei", Università di Padova, I-35131 Padova, Italy
12. Department of Physics, Center for Cosmology and Astro-Particle Physics, The Ohio State University, Columbus, OH 43210, USA
13. Combined Array for Research in Millimeter-wave Astronomy (CARMA), Big Pine, CA 93514, USA

14. Radio Astronomy Laboratory, University of California, Berkeley, CA 94720, USA

15. Istituto Nazionale di Fisica Nucleare, Sezione di Perugia, I-06123 Perugia, Italy

16. Dipartimento di Fisica, Università degli Studi di Perugia, I-06123 Perugia, Italy

17. Dipartimento di Fisica "M. Merlin" dell'Università e del Politecnico di Bari, I-70126 Bari, Italy

18. Istituto Nazionale di Fisica Nucleare, Sezione di Bari, 70126 Bari, Italy

19. Laboratoire Leprince-Ringuet, École polytechnique, CNRS/IN2P3, Palaiseau, France

20. Department of Physics, University of Washington, Seattle, WA 98195-1560, USA

21. Institut de Ciencies de l'Espai (IEEC-CSIC), Campus UAB, 08193 Barcelona, Spain

22. INAF-Istituto di Astrofisica Spaziale e Fisica Cosmica, I-20133 Milano, Italy

23. Agenzia Spaziale Italiana (ASI) Science Data Center, I-00044 Frascati (Roma), Italy

24. NASA Goddard Space Flight Center, Greenbelt, MD 20771, USA

25. Center for Research and Exploration in Space Science and Technology (CRESST) and NASA Goddard Space Flight Center, Greenbelt, MD 20771, USA

26. Department of Physics and Center for Space Sciences and Technology, University of Maryland Baltimore County, Baltimore, MD 21250, USA

27. George Mason University, Fairfax, VA 22030, USA

28. Laboratoire de Physique Théorique et Astroparticules, Université Montpellier 2, CNRS/IN2P3, Montpellier, France

29. Max-Planck Institut für extraterrestrische Physik, 85748 Garching, Germany

30. Department of Physics and Astronomy, Sonoma State University, Rohnert Park, CA 94928-3609, USA

31. Department of Physics, Stockholm University, AlbaNova, SE-106 91 Stockholm, Sweden

32. Royal Swedish Academy of Sciences Research Fellow, funded by a grant from the K. A. Wallenberg Foundation

33. Institut universitaire de France, 75005 Paris, France

34. Dipartimento di Fisica, Università di Udine and Istituto Nazionale di Fisica Nucleare, Sezione di Trieste, Gruppo Collegato di Udine, I-33100 Udine, Italy

35. CNRS/IN2P3, Centre d'Études Nucléaires Bordeaux Gradignan, UMR 5797, Gradignan, 33175, France

36. Université de Bordeaux, Centre d'Études Nucléaires Bordeaux Gradignan, UMR 5797, Gradignan, 33175, France

37. Osservatorio Astronomico di Trieste, Istituto Nazionale di Astrofisica, I-34143 Trieste, Italy

38. Max-Planck-Institut für Radioastronomie, Auf dem Hügel 69, 53121 Bonn, Germany

39. Department of Physical Sciences, Hiroshima University, Higashi-Hiroshima, Hiroshima 739-8526, Japan

40. Department of Astronomy and Astrophysics, Pennsylvania State University, University Park, PA 16802, USA

41. Department of Physics and Department of Astronomy, University of Maryland, College Park, MD 20742, USA

42. INAF Istituto di Radioastronomia, 40129 Bologna, Italy

43. Center for Space Plasma and Aeronomic Research (CSPAR), University of Alabama in Huntsville, Huntsville, AL 35899, USA

44. Department of Physics, Royal Institute of Technology (KTH), AlbaNova, SE-106 91 Stockholm, Sweden

45. Dr. Remeis-Sternwarte Bamberg, Sternwartstrasse 7, D-96049 Bamberg, Germany

46. Erlangen Centre for Astroparticle Physics, D-91058 Erlangen, Germany

47. Universities Space Research Association (USRA), Columbia, MD 21044, USA

48. Research Institute for Science and Engineering, Waseda University, 3-4-1, Okubo, Shinjuku, Tokyo, 169-8555 Japan

49. Department of Physics, Tokyo Institute of Technology, Meguro City, Tokyo 152-8551, Japan

50. Cosmic Radiation Laboratory, Institute of Physical and Chemical Research (RIKEN), Wako, Saitama 351-0198, Japan

51. Centre d'Étude Spatiale des Rayonnements, CNRS/UPS, BP 44346, F-30128 Toulouse Cedex 4, France

52. ICRAR/Curtin Institute of Radio Astronomy, Bentley WA 6102., Australia

53. Cahill Center for Astronomy and Astrophysics, California Institute of Technology, Pasadena, CA 91125, USA

54. Istituto Nazionale di Fisica Nucleare, Sezione di Roma "Tor Vergata", I-00133 Roma, Italy

55. Department of Physics and Astronomy, University of Denver, Denver, CO 80208, USA

56. Department of Physics, Graduate School of Science, University of Tokyo, 7-3-1 Hongo, Bunkyo-ku, Tokyo 113-0033, Japan

57. Santa Cruz Institute for Particle Physics, Department of Physics and Department of Astronomy and Astrophysics, University of California at Santa Cruz, Santa Cruz, CA 95064, USA

58. Institut für Astro- und Teilchenphysik and Institut für Theoretische Physik, Leopold-Franzens-Universität Innsbruck, A-6020 Innsbruck, Austria

59. Kavli Institute for Cosmological Physics, University of Chicago, Chicago, IL 60637, USA

60. Space Sciences Division, NASA Ames Research Center, Moffett Field, CA 94035-1000, USA

61. NYCB Real-Time Computing Inc., Lattingtown, NY 11560-1025, USA

62. Department of Chemistry and Physics, Purdue University Calumet, Hammond, IN 46323-2094, USA

63. Institute of Space and Astronautical Science, JAXA, 3-1-1 Yoshinodai, Sagamihara, Kanagawa 229-8510, Japan

64. University of New Mexico, MSC07 4220, Albuquerque, NM 87131, USA

65. Partially supported by the International Doctorate on Astroparticle Physics (IDAPP) program

66. Institució Catalana de Recerca i Estudis Avançats (ICREA), Barcelona, Spain

67. Consorzio Interuniversitario per la Fisica Spaziale (CIFS), I-10133 Torino, Italy

68. Dipartimento di Fisica, Università di Roma "Tor Vergata", I-00133 Roma, Italy

69. Space Science Institute, Boulder, CO 80301, USA

70. School of Pure and Applied Natural Sciences, University of Kalmar, SE-391 82 Kalmar, Sweden

71. Instituto de Astrofisica de Andalucía, CSIC, 18080 Granada, Spain

72. Department of Astronomy, University of Michigan, Ann Arbor, MI 48109-1042, USA

73. Pulkovo Observatory, 196140 St. Petersburg, Russia

74. Instituto de Astronomía, Universidad Nacional Autónoma de México, CP 04510 México, D. F., México

75. Tuorla Observatory, University of Turku, FI-21500 Piikkiö, Finland

76. Department of Physics and Astronomy, Ohio University, Athens, OH 45701, USA

77. Osservatorio Astrofisico di Catania, 95123 Catania, Italy

78. Graduate Institute of Astronomy, National Central University, Jhongli 32054, Taiwan

79. INAF-Osservatorio Astronomico di Collurania, 64100 Teramo, Italy

80. Astronomical Institute, St. Petersburg State University, St. Petersburg, Russia

81. Cavendish Laboratory, Cambridge CB3 0HE, UK

82. Harvard-Smithsonian Center for Astrophysics, Cambridge, MA 02138, USA

83. Landessternwarte, Universität Heidelberg, Königstuhl, D 69117 Heidelberg, Germany

84. Instituto de Astronomía, Universidad Nacional Autónoma de México, CP 22860 Ensenada, B. C., México

85. Aalto University Metsähovi Radio Observatory, FIN–02540 Kylmälä, Finland

86. Institute for Astrophysical Research, Boston University, Boston, MA 02215, USA

87. Hiroshima Astrophysical Science Center, Hiroshima University, Higashi-Hiroshima, Hiroshima 739-8526, Japan

88. Department of Physics and Astrophysics, Nagoya University, Chikusa-ku Nagoya 464-8602, Japan

89. Abastumani Observatory, Mt. Kanobili, 0301 Abastumani, Georgia

90. School of Physics and Astronomy, University of Southampton, Southampton SO17 BJ, UK

91. Nicolaus Copernicus Astronomical Center, 00-716 Warsaw, Poland

92. Osservatorio Astronomico di Roma, 00040 Monte Porzio Catone, Italy

93. INAF, Osservatorio Astronomico di Torino, I-10025 Pino Torinese (TO), Italy

94. Astrophyisikalisches Institut Potsdam, Potsdam, Germany

95. Astronomical Observatory, Jagiellonian University, 30-244 Kraków, Poland

It is widely accepted that strong and variable radiation detected over all accessible energy bands in a number of active galaxies arises from a relativistic, Doppler-boosted jet pointing close to our line of sight[1]. The size of the emitting zone and the location of this region relative to the central supermassive black hole are, however, poorly known, with estimates ranging from light-hours to a light-year or more. Here we report the coincidence of a gamma (γ)-ray flare with a dramatic change of optical polarization angle. This provides evidence for co-spatiality of optical and γ-ray emission regions and indicates a highly ordered jet magnetic field. The results also require a non-axisymmetric structure of the emission zone, implying a curved trajectory for the emitting material within the jet, with the dissipation region located at a considerable distance from the black hole, at about 10^5 gravitational radii.

The flat spectrum radio quasar 3C 279 was the first bright γ-ray blazar reported by the EGRET instrument aboard the Compton Gamma-Ray Observatory to show strong and rapidly variable γ-ray emission[2–4]; recently, it also has been detected at photon energies above 100 GeV by the MAGIC ground-based Cherenkov telescope[5]. This blazar, at the redshift $z = 0.536$, harbors a black hole with mass[6,7] $M \simeq (3-8) \times 10^8 M_\odot$ (where $M_\odot$ is the mass of the Sun); for specificity, we adopt $6 \times 10^8 M_\odot$. It shows superluminal expansion best described as the jet material propagating with the bulk Lorentz factor $\Gamma_{\rm jet} = 16 \pm 3$ at a small angle ($\theta \sim 2^\circ$) to our line of sight[8]. The high degree of the optical polarization provides evidence for the presence of a well ordered magnetic field in the emission zone[9]. This may

reflect either the global topology of the large-scale magnetic field, or may result from the compression of chaotic magnetic fields in shocks and shear regions along the outflow[10].

The best coverage of the broad-band flux variability of 3C 279 has been obtained after the start of routine scientific operation of the Large Area Telescope (LAT)[11] onboard of the recently launched *Fermi* Gamma-ray Space Telescope (August 4th 2008 = 54682 Modified Julian Day, or MJD). In Figure 1 we plot the flux history in the γ-ray band above 200 MeV, as well as in the X-ray, optical, infrared, and radio bands together with polarization information in the optical band. Among all the observed bands, the γ-ray band shows the most violent variations, with a change by an order of magnitude in flux during the observation. It also dominates the electromagnetic output of 3C 279, with the apparent γ-ray luminosity as much as $\sim 10^{48}$ erg s^{-1} (see Figure 2 and ref. 3, 4). After being in the quiescent state for the first 100 days or so, the γ-ray flux starts to increase at $\sim$ 54780 MJD, but without any significant spectral changes: the γ-ray photon index is relatively constant during the entire observed period. The high γ-flux state persists for $\sim$ 120 days and is associated with erratic flaring, accompanied by bright and variable optical emission.

Towards the end of the high-flux state there is a sharp γ-ray flare at 54880 MJD with a doubling timescale of as short as 1 day. This sharp γ-ray flare coincides with a significant drop of the level of optical polarization (polarization degree: PD), from $\sim$ 30% down to a few per cent, lasting for $\Delta t \sim 20$ days. Subsequently, both γ-ray and optical fluxes gradually decrease together and reach the quiescent level, followed by a temporary recovery of the high degree of polarization. This event is associated with a dramatic change of the electric vector position angle (EVPA) of the polarization, in contrast to being relatively constant before the event at $\sim 50^\circ$ (parallel to the jet direction observed by Very Long Baseline Interferometry observations in radio bands; see ref. 8 for example). Because the EVPA has $\pm 180^\circ \times n$ (where $n = 1, 2...$) ambiguity, we selected values on the assumption of a smooth change of the EVPA, such that it would follow the overall trend. The polarization angle increases slightly at 54880 MJD – coincident with the γ-ray flare – then decreases by 208° with a rate of $\sim 12^\circ$ per day, and returns to a level nearly exactly 180° from the original level, resembling closely the behavior of optical polarization measured in BL Lacertae[12], but at a rate four times slower. This clearly indicates that the sharp γ-ray flare is unambiguously correlated with the dramatic change of optical polarization due to a single, coherent event, rather than a superposition of multiple but causally unrelated, shorter duration events.

Concurrent X-ray observations indicate a relatively steady X-ray flux during the high γ-ray flux state (although with modest amplitude variations roughly mirroring the γ-ray time series; A. Marscher, priv. comm.), but reveal a significant, symmetrical flare about 60 days after the second γ-ray peak — at 54950 MJD — with duration of $\sim$ 20 days, similar

to the duration of the γ-ray flare. It suggests the X-ray photons are produced at a distance from the black hole comparable to the distance of the optical/γ-ray photons. Importantly, this X-ray flare is accompanied only by a modest increase of optical activity and not by a prominent optical or γ-ray flare. The X-ray spectrum during the isolated flare remains much harder than the optical spectrum (see Figure 2), and therefore cannot be attributed to a temporary extension of the high-energy tail of the synchrotron emission, but instead, may be generated by inverse-Compton scattering of low-energy electrons. However, the similarity of profiles of the γ-ray and X-ray flares argues against the latter being just a delayed version of the former due to, e.g., particle cooling. Therefore, the X-ray flare must be produced independently by another mechanism involving primarily lower energy electrons.

During the entire multiwavelength campaign reported here, the radio and millimeter fluxes are less variable than fluxes in other bands. In particular, they stay nearly constant in the periods of the two prominent γ-ray flares and the isolated X-ray flare, and no associated or delayed radio flare was observed. This suggests that the blazar activity in 3C 279 takes place where the synchrotron radiation at these wavelengths is not yet fully optically thin, constraining the transverse size $R_{\rm blazar}$ of the blazar emission zone[13]

$$R_{\rm blazar} < 5{\times}10^{16}\,(\nu F_\nu/2{\times}10^{-11}\,{\rm erg\,cm^{-2}\,s^{-1}})^{1/2}\,(B'/0.3\,{\rm G})^{1/4}\,(\nu/10^{11.5}\,{\rm Hz})^{-7/4}\,(\Gamma_{\rm jet}/15)^{-1/4}\,{\rm cm}$$

(where νF_ν is the energy flux measured in the millimeter band [$\sim 10^{11.5}$ Hz]), which is consistent with the limit provided by shortest doubling timescales of the γ-ray flux variations.

The gradual rotation of the polarization angle is unlikely to originate in a straight, uniform axially symmetric, matter-dominated jet because any compression of the jet plasma by, for example, a perpendicular shock moving along the jet and viewed at a small but constant angle to the jet axis would change the degree of polarization, but would not result in a gradual change of EVPA. Instead, it can reflect a non-axisymmetric magnetic field distribution (as in, for example, ref. 14), a swing of the jet across our line of sight (which in turn does not require any source/pattern propagation), or a curved trajectory of the dissipation/emission pattern. The last possibility may be due to propagation of an emission knot following a helical path in a magnetically dominated jet as was recently investigated in the context of the optical polarization event seen in BL Lacertae[12] or may involve the "global" bending of a jet. The magnetic field in the emission region is anisotropic (presumably concentrated in the plane of a shock or disturbance propagating along the jet), so the degree and angle of observed polarization then depends on the instantaneous angle θ of the direction of motion of the radiating material to the line of sight. The maximum rotation rate of the polarization angle would correspond to $\theta = \theta_{\rm min}$ and polarization degree would be highest for $\theta \sim 1/\Gamma_{\rm jet}$.

The "bent jet" scenario can explain the observed polarization event (the change of the angle as well as the magnitude of polarization) provided the jet curvature is confined to the plane inclined to the line of sight at an angle $\theta_{\rm min} < 1/\Gamma_{\rm jet}$ and configured in such a way that the jet trajectory projected on the sky turns by almost 180°. Similar geometry - albeit on larger scales - has been observed in another blazar, PKS 1510-089 (ref. 15). Nonetheless, in both scenarios, the coherent polarization event is produced by a density pattern co-moving along the jet, and therefore, it is possible to estimate the distance traveled by the emitting material during the flare $\Delta r_{\rm event}$; this in turn allows us to constrain the distance $r_{\rm event}$ of the dissipation region (where flaring occurs) from the black hole, because $r_{\rm event} \geq \Delta r_{\rm event}$. With this, $r_{\rm event} \geq \Delta r_{\rm event} \sim 10^{19}\,(\Delta t_{\rm event}/20\,{\rm days})\,(\Gamma_{\rm jet}/15)^2\,{\rm cm}$, which is ~ 5 orders of magnitude larger than the gravitational radius of the black hole in 3C 279.

The constraints on the distance of the dissipation region can be relaxed under "flow-through" scenarios, in where the emission patterns may move much more slowly than the bulk speed of the jet or not propagate at all: one such example is the model involving swings ("wobbling") of the jet associated with jet instabilities such that its boundary moves relative to our line of sight. In this case, the timescale for the observed variation is the timescale for the jet motion. Consequently, the emission region easily can be much closer (by a factor $\Gamma_{\rm jet}^2$) to the black hole than in the "helical" or "bent jet" scenarios, because the natural radial scale for $\Delta t_{\rm event} \sim 20$ days is $r_{\rm event} \sim c\Delta t_{\rm event} \sim 500 - 1000$ gravitational radii (see, e.g., ref. 16). Under this scenario, the angle the jet makes with the line of sight must change by at least $\sim \Gamma_{\rm jet}^{-1}$ in order to explain the large swing of polarization. Here, the jet motion can be imposed at its base, be caused by deflection due to external medium, or be a consequence of dynamical instability.

This leaves us with three viable possibilities. Both the scenario involving a knot propagating along the helical magnetic field lines and the "flow-through" scenario above imply that the rotation of the polarization angle should be preferentially following the same direction, because in those two models the twist presumably originates in the inner accretion disk. In our case, we observe the rotation of the polarization angle to be opposite in direction to that measured previously[9], leaving us with the "bent jet" model combined with a small swing of the jet as the most compelling scenario.

The dominant source of "seed" photons for inverse-Compton scattering depends on the distance of the dissipation event from the central black hole[17]. At the parsec distances predicted by the "helical" or "bent jet" scenarios involving the radiating material co-moving with the jet, the "seed" radiation fields are dominated by infrared radiation emitted by a warm dust located in the circumnuclear molecular torus and by synchrotron radiation produced within the jet. At sub-parsec distances implied by the "flow-through" scenarios,

this photon field can be the broad emission line region[13] (clearly detected in this object[18], as expected in a quasar possessing a luminous accretion disk[19]), as well as the direct radiation of such a disk[20] or its corona[21]. In any case, the ~ 20 GeV electrons and positrons producing the highest-energy γ rays and the polarized optical radiation lose their energy on timescales shorter than the light travel time from the black hole, and so must be accelerated locally.

In summary, the close association of the energetically dominant γ-ray flare with the smooth, continuous change of the optical polarization angle suggests co-spatiality of the optical and γ–ray emission and provides evidence for the presence of highly ordered magnetic fields in the regions of the γ–ray production. Provided the emission pattern is co-moving with the jet, we can measure the distance of the coherent event to be of the order of 10^5 gravitational radii away from the black hole. While the available data cannot exclude the theoretically less explored "flow-through" scenarios - where the dissipation events may take place at much smaller distances, down to $\sim 10^3$ gravitational radii - the opposite direction of rotation of the optical polarization angle than previously measured appears to support the jet bending at larger distances as the best explanation of the available data. Furthermore, the detection of the isolated X-ray flare challenges the simple, one-zone emission models, rendering them too simple. Regardless, the *Fermi* satellite has been in operation for only just over a year, and the outlook for a more comprehensive picture of these enigmatic objects, primarily via multi-band campaigns including well-sampled optical polarimetry, is excellent.

References

[1] Ulrich, M-H, Maraschi, L. & Urry, C. M. Variability of Active Galactic Nuclei *Ann. Rev. Astron. Astrophys.*, **35**, 445–502 (1977)

[2] Hartman, R. C., *et al.* Detection of High-energy Gamma Radiation from Quasar 3C 279 by the EGRET Telescope on the Compton Gamma Ray Observatory. *Astrophys. J. (Lett.)*, **385**, L1–L4 (1992).

[3] Kniffen, D. A., *et al.* Time Variability in the gamma-ray Emission of 3C 279. *Astrophys. J.*, **411**, 133–136 (1994).

[4] Wehrle, A. E., *et al.* Multiwavelength Observations of a Dramatic High-Energy Flare in the Blazar 3C 279. *Astrophys. J.*, **497**, 178–187 (1998).

[5] Albert, J., *et al. (The MAGIC collaboration)* Very-High-Energy Gamma-rays from a Distant Quasar: How Transparent Is the Universe? *Science*, **320**, 1752–1754 (2008).

[6] Nilsson, K., *et al.* The Host Galaxy of 3C 279. *Astron. Astrophys.*, **505**, 601–604, (2009)

[7] Woo, J.-H. & Urry, C. M. Active Galactic Nucleus Black Hole Masses and Bolometric Luminosities. *Astrophys. J.*, **579**, 530–544 (2002).

[8] Jorstad, S. G., *et al.* Polarimetric Observations of 15 Active Galactic Nuclei at High Frequencies: Jet Kinematics from Bimonthly Monitoring with the Very Long Baseline Array. *Astron. J.*, **130**, 1418–1465 (2005).

[9] Larionov, V. M., *et al.* Results of WEBT, VLBA and RXTE Monitoring of 3C 279 during 2006-2007. *Astron. Astrophys.* **492**, 389–400 (2008).

[10] Laing, R. A. A Model for the Magnetic-field Structure in Extended Radio Sources. *Mon. Not. R. Astron. Soc.* **193**, 439–449 (1980).

[11] Atwood, W. B., *et al. (The Fermi-LAT collaboration)* The Large Area Telescope on the Fermi Gamma-Ray Space Telescope Mission. *Astrophys. J.*, **697**, 1071–1102 (2009).

[12] Marscher, A. P., *et al.* The Inner Jet of an Active Galactic Nucleus as Revealed by a Radio-to-Gamma-ray Outburst. *Nature*, **452**, 966–969 (2008).

[13] Sikora, M., Begelman, M. C. & Rees, M. J. Comptonization of Diffuse Ambient Radiation by a Relativistic Jet: the Source of Gamma-rays from Blazars? *Astrophys. J.*, **421** 153–162 (1994).

[14] Konigl, A. & Choudhuri, A. R. A model of the Polarization Position-angle Swings in BL Lacertae Objects. *Astrophys. J.* **289**, 188–192 (1985).

[15] Homan, D. C., *et al.* PKS 1510-089: A Head-On View of a Relativistic Jet. *Astrophys. J.*, **580**, 742–748 (2002).

[16] Lyutikov, M., Pariev, V. I., & Blandford, R. Polarization of Prompt Gamma-ray Burst Emission: Evidence for Electromagnetically Dominated Outflow. *Astrophys. J.* **597**, 998–1009 (2003)

[17] Sikora, M., Stawarz, L., Moderski, R., Nalewajko, K. & Madejski, G. Constraining Emission Models of Luminous Blazar Sources. *Astrophys. J.*, **704**, 38–50 (2009).

[18] Netzer, H., *et al.* The Optical-Ultraviolet-gamma-ray Spectrum of 3C 279. *Astrophys. J.*, **430**, 191–195 (1994).

[19] Pian, E., *et al.* Ultraviolet and Multiwavelength Variability of the Blazar 3C 279: Evidence for Thermal Emission. *Astrophys. J.*, **521**, 112–120 (1999).

[20] Dermer, C., Schlickheiser, R., & Mastichiadis, A. Gamma-rays from Extragalactic radio sources. *Astron. Astrophys.*, **256**, L27–L30 (1992).

[21] Blandford, R. D. & Levinson, A. Pair Cascades in Extragalactic Jets: 1: Gamma-rays. *Astrophys. J.*, **441**, 79–95 (1995).

[22] Abdo, A. A., *et al. (The Fermi-LAT collaboration)* Early Fermi Gamma-ray Space Telescope Observations of the Quasar 3C 454.3. *Astrophys. J.*, **699**, 817–823 (2009).

[23] Villata, M., *et al.* The correlated optical and radio variability of BL Lacertae. WEBT data analysis 1994-2005. *Astron. Astrophys.* **501**, 455–460 (2009).

[24] Watanabe, M., *et al.* TRISPEC: A Simultaneous Optical and Near-Infrared Imager, Spectrograph, and Polarimeter. *Pub. Astron. Soc. Pacif.*, **117**, 870–884 (2005).

[25] Fuhrmann, L., Zensus, J. A., Krichbaum, T. P., Angelakis, E., & Readhead, A. C. S. Simultaneous Radio to (Sub-) mm-Monitoring of Variability and Spectral Shape Evolution of potential GLAST Blazars. *The First GLAST Symposium. AIP Conference Proceedings*, **921**, 249–251 (2007)

Acknowledgments: The *Fermi*-LAT Collaboration acknowledges support from a number of agencies and institutes for both development and the operation of the LAT as well as scientific data analysis. These include NASA and DOE in the United States, CEA/Irfu and IN2P3/CNRS in France, ASI and INFN in Italy, MEXT, KEK, and JAXA in Japan, and

the K. A. Wallenberg Foundation, the Swedish Research Council and the National Space Board in Sweden. Additional support from INAF in Italy for science analysis during the operations phase is also gratefully acknowledged. The GASP-WEBT observatories participating in this work are Abastumani, Calar Alto, Campo Imperatore, Crimean, Kitt Peak (MDM), L'Ampolla, Lowell (Perkins-PRISM), Lulin, Roque de los Muchachos (KVA and Liverpool), San Pedro Mártir, St. Petersburg for the optical-NIR bands, and Mauna Kea (SMA), Medicina, Metsahovi, Noto and UMRAO for the mm-radio band, and are supported in part by the Georgian National Science Foundation, the Spanish "Ministerio de Ciencia e Innovación", the NSF and NASA and the Smithsonian Institution in the United States, the UK Science and Technology Facilities Council, the Academia Sinica in Taiwan, the Russian RFBR and the Academy of Finland. M. Hayashida is supported by the JSPS for the Postdoctoral Fellowship for Research Abroad.

Author Contributions: All authors contributed to the work presented in this paper. The Kanata observations and data analysis were led by M. Uemura and R. Itoh. M. Villata organized the optical-radio observations by GASP-WEBT as the president of the collaboration.

Author Information: Correspondence and requests for materials should be addressed to M. Hayashida (mahaya@slac.stanford.edu) and G. Madejski (madejski@slac.stanford.edu)

Figure Legends

Figure 1: History of flux in various bands, γ-ray photon index, and optical polarization of 3C 279. Light curves at the indicated wave bands covering 1 year since the Modified Julian Day (MJD) of 54650 (corresponding to July 3rd 2008). The two dashed vertical lines indicate 54880 and 54900 MJD. Error bars at each point represent a ± 1 s.d. statistical uncertainty. **a-b,** Gamma-ray flux F_γ and photon index Γ above 200 MeV averaged over 3-day intervals as measured by *Fermi*-LAT based on photons that passed the "diffuse" event selection. The source fluxes are calculated using "P6_V3_DIFFUSE" for the instrumental response function and a simple power-law spectral model ($\mathrm{d}F/\mathrm{d}E \propto E^{-\Gamma}$). The detailed data analysis procedures are analogous to those in ref. 22. **c,** X-ray integrated flux F_X between 2 and 10 keV, calculated by fitting the data with the simple power-law model taking into account a Galactic absorption. Light-green points are from the observations with the Proportional Counter Array (PCA) on-board the Rossi X-ray Timing Explorer (*RXTE*) and dark green points are measurements by *Swift*-XRT. **d,** Optical and ultra-violet (UV) fluxes in several bands. R-band data were taken by ground-based telescopes from the GASP-WEBT collaboration[23]. V-band data were taken by a ground-based telescope (Kanata-TRISPEC[24]) and *Swift*-UVOT. Data in all other bands were acquired by *Swift*-UVOT. **e-f,** Polarization degree (PD) and electric vector position angle (EVPA) of the optical polarization measured by the Kanata-TRISPEC in the V-band (dark blue) and by the KVA telescope without any filters (light blue). Note that EVPA has $\pm 180^\circ \times n$ (where $n = 1, 2...$) ambiguity. The horizontal dashed lines in **f** refer to EVPA of $50^\circ$and -130°. **g-h,** Near-infrared (NIR) and radio fluxes measured by ground-based telescopes (Kanata-TRISPEC [J, K_s], OVRO [15 GHz] and GASP-WEBT [J, H, K and several millimeter and radio bands]). All UV, optical and NIR data are corrected for the Galactic absorption.

Figure 2: Energy spectrum from radio to γ-ray band of 3C 279 at two different epochs. The red points were taken between 54880 and 54885 MJD, corresponding to the first five days of the sharp γ-ray flare accompanying the dramatic polarization change event [epoch-1]. The blue points were taken between 54950 and 54960 MJD, around the peak of the isolated X-ray flare [epoch-2]. The γ-ray spectra were measured by *Fermi*-LAT. In the X-ray band, the flux points are obtained by the *RXTE*-PCA in the epoch-1 (red) and by *Swift*-XRT in the epoch-2 (blue). The fluxes in the UV range were measured by *Swift*-UVOT. Observations in the optical-to-radio bands were performed by ground-based telescopes as given in Figure 1 (with additional radio coverage provided by the Effelsberg radio telescope[25]). Each data point represents an average source flux and the error bar represents ± 1 s.d. of the flux during each epoch. Each data point is already corrected for Galactic absorption. Note that the total energy associated with the X-ray flare is relatively modest, about 30 times less than the energy associated with the γ-ray flare accompanying

the dramatic polarization change, and the γ-ray emission is still dominant, having five times the X-ray energy flux even during the X-ray flare event.

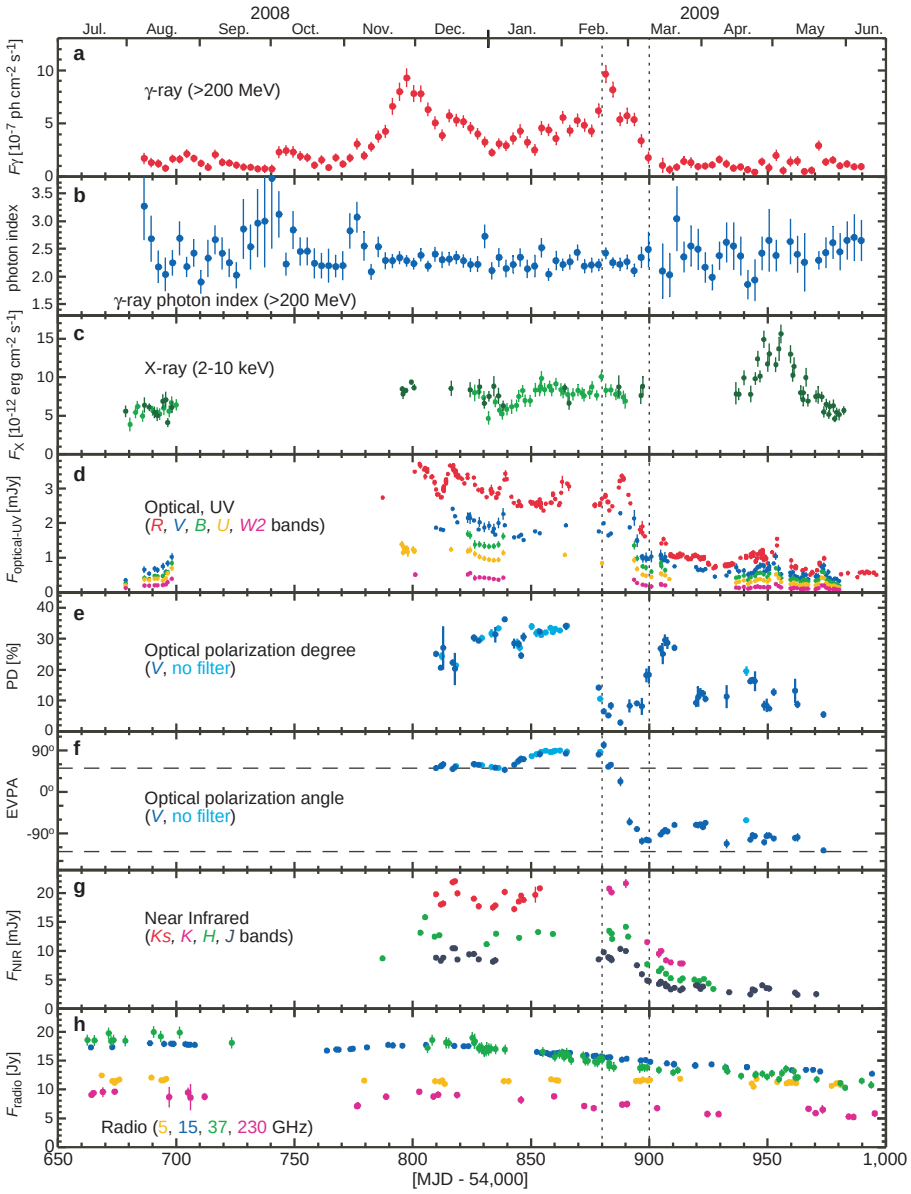
2008
2009
Jul.
Aug.
Sep.
Oct.
Nov.
Dec.
Jan.
Feb.
Mar.
Apr.
May
Jun.
a
γ-ray (>200 MeV)
F_γ [10^{-7} ph cm^{-2} s^{-1}]
b
γ-ray photon index (>200 MeV)
photon index
c
X-ray (2-10 keV)
F_X [10^{-12} erg cm^{-2} s^{-1}]
d
Optical, UV
(R, V, B, U, W2 bands)
$F_{optical-UV}$ [mJy]
e
Optical polarization degree
(V, no filter)
PD [%]
f
Optical polarization angle
(V, no filter)
EVPA
g
Near Infrared
(Ks, K, H, J bands)
F_{NIR} [mJy]
h
Radio (5, 15, 37, 230 GHz)
F_{radio} [Jy]
650
700
750
800
850
900
950
1,000
[MJD - 54,000]

Figure 1:

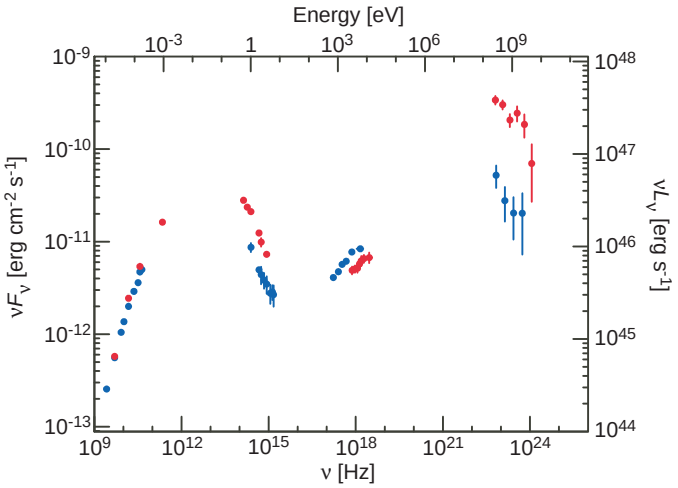
Energy [eV]
10^-3
1
10^3
10^6
10^9
10^-9
10^-10
10^-11
10^-12
10^-13
νF_ν [erg cm^-2 s^-1]
10^48
10^47
10^46
10^45
10^44
νL_ν [erg s^-1]
10^9
10^12
10^15
10^18
10^21
10^24
ν [Hz]

Figure 2: